AGRICULTURE

# Underestimated agricultural losses due to flooding

**Shulei Zhang[1]*, Liming Zhou[2], Hongbin Liang[1], Omarjan Obulkasim[1], Yongjiu Dai[1]***



**Flooding poses a growing threat to global food security in a warming climate, yet a critical gap remains in quantifying flood-induced agricultural losses, hindering the design of effective adaptations to potential food crises. Here, we present a methodological framework for projecting crop losses from flooding, using a flooding stress algorithm to refine yield simulations from existing crop models. This approach ensures that simulated yield reductions for maize, soybean, and wheat align with observations in the United States and demonstrates strong agreement between estimated and reported flood-induced crop losses both in the United States and globally. Future flood-induced losses, which were substantially underestimated in the original simulations, are projected to be comparable to or even exceed drought-induced losses in many regions and exhibit distinct spatial and temporal patterns. Mitigation of greenhouse gas emissions helps reduce these risks. This framework provides a robust basis for assessing agricultural vulnerability to flood shocks and guiding strategies to safeguard food supplies under climate change.**

## INTRODUCTION

Floods are among the most destructive natural disasters, with severe consequences for agriculture (*1*–*6*). Field experiments (*7*–*9*) and national surveys (*10*) consistently report crop yield losses from flooding (*11*). According to the Food and Agriculture Organization (FAO), floods rank as the second gravest agricultural disaster worldwide, affecting ~27% of cultivated lands annually, with the potential to destabilize food systems and threaten food security from local to global scales (*5*, *6*, *12*, *13*). Rising food demand and increasing flood risks under climate change (*14*–*16*) heighten the urgency of strengthening agricultural resilience.

Robust projections of the impacts of natural disasters on crop yield, grounded in process-based models, represent an important and indispensable path to identifying adaptation priorities in response to potential food crises (*17*–*19*). However, most previous assessments and projections have focused on drought, heat, $CO_2$ effects, or other gradual climate changes, rather than on flooding (*20*–*23*). A major obstacle is the nascent stage of representing flood impacts on crop yield in these models (*13*). Specifically, this requires effective parameterizations in two key areas: accurately capturing flood dynamics on one hand and quantifying their specific effects on crop growth on the other. The first task is particularly challenging as most crop models are developed to simulate crop growth processes rather than hydrological processes (*24*–*26*). The second task has advanced rapidly in recent years, with some crop models incorporating parameterizations of flooding and/or waterlogging effects on crop growth processes, such as phenology, photosynthesis, root growth, nitrogen uptake, and grain formation (*7*, *12*, *27*–*30*). However, quantitatively representing these processes from a bottom-up perspective remains challenging due to the complexity of schemes and parameters that rely heavily on field experiment data for specific processes. Consequently, such modeling efforts are often tailored to specific crops or regional studies (*7*, *12*, *27*–*30*). These limitations hinder the capacity to predict flood impacts across diverse crops and broad spatial scales (*13*, *31*), which is critical for providing robust scientific guidance on potential agricultural losses.

To bridge this knowledge gap and strengthen the adaptive capacity of the global food system to flooding, we develop a modeling framework for estimating global crop losses due to floods. This framework integrates state-of-the-art crop and flood modeling through a crop flooding stress algorithm, which quantifies the comprehensive effects of flooding on crops in a generalized yet effective manner, resulting in adjusted crop model outcomes that align well with observed yield reductions. Observed yield changes were derived from data on maize, soybean, and wheat, the three most widely cultivated crops in the United States. We then estimated the economic losses associated with flood-induced yield reductions for the three crops and compared these estimates with the indemnities for flood damages provided by the US Department of Agriculture (USDA) and with global flood-induced losses reported by the Emergency Events Database (EM-DAT) to verify the robustness of our estimates. Last, we projected potential flood-induced losses for maize, soybean, and wheat, along with their temporal change patterns under various emission scenarios, using global yield and runoff simulations under future climate change.

## RESULTS

### Yield response to flooding

We investigated the observed response of crop yield to water availability anomalies in the continental United States. The percentage change in yield for each county-year sample was calculated as the ratio of the yield anomaly (i.e., the difference between actual and trend yield) to the trend yield. The yield changes were then aggregated by bins of precipitation anomaly to derive the yield response curve to extremes in water availability (see Materials and Methods for details). As shown by the black solid lines in Fig. 1, yield losses occurred when water availability deviated from the norm. When water availability was insufficient, crops experienced drought stress and impaired growth. Conversely, excessive rainfall caused flooding through land surface runoff and routing processes (fig. S5), leading to waterlogged conditions that adversely affected crops and reduced yield. In both cases, losses intensified with the severity of drought

[1]Southern Marine Science and Engineering Guangdong Laboratory (Zhuhai), Guangdong Province Key Laboratory for Climate Change and Natural Disaster Studies, School of Atmospheric Sciences, Sun Yat-sen University, Zhuhai, Guangdong, China. [2]Department of Atmospheric and Environmental Sciences, University at Albany, State University of New York, Albany, NY, USA.
*Corresponding author. Email: zhangshlei@mail.sysu.edu.cn (S.Z.); daiyj6@mail.sysu.edu.cn (Y.D.)

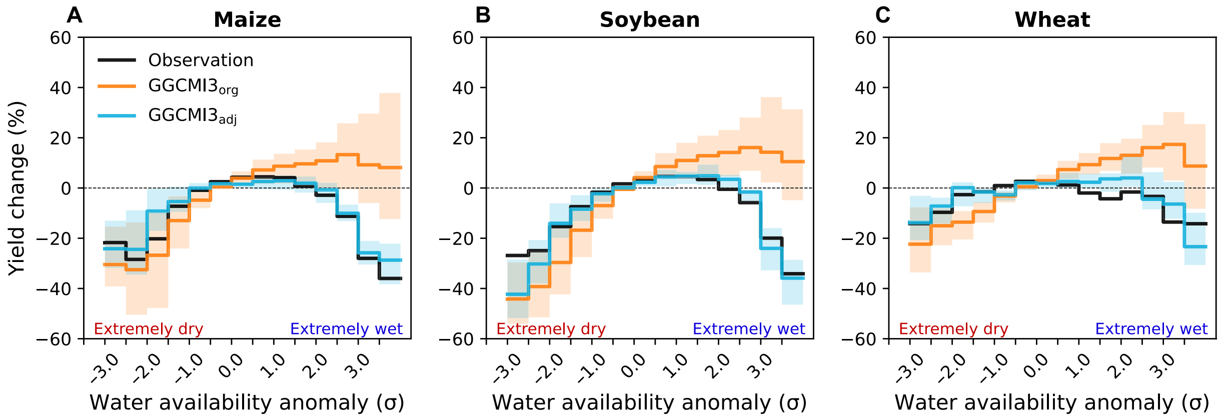


**Fig. 1. Observed and simulated crop yield responses to water availability anomalies in the continental United States.** (**A**) Observed maize yield response to water availability anomaly (black solid line) compared with the original GGCMI3 simulations (GGCMI3$_{org}$; orange solid line and shaded area) and the adjusted GGCMI3 simulations accounting for flooding impacts (GGCMI3$_{adj}$; blue solid line and shaded area). The orange and blue solid lines represent multimodel median responses, and the shaded areas indicate the interquartile range across models. (**B** and **C**) Same as (A) but for soybean and wheat, respectively.

and/or flooding. Together, these two types of stress ranked among the top causes of crop losses in the United States (fig. S1).

The ensemble median outcomes of global crop models participating in Phase 3 of the Global Gridded Crop Model Intercomparison Project (GGCMI3) captured the general negative yield responses to extreme dry conditions, indicating that the models represent drought stress to a reasonable extent (illustrated by the orange solid lines). However, the GGCMI3 crop models failed to capture the observed yield reductions under extreme wet conditions, with biases as high as 26.7, 28.3, and 21.3% for maize, soybean, and wheat, respectively (Fig. 1). This is mainly due to the models' lack of consideration for crop damage caused by flooding, leading to substantial overestimation of yields under extreme wet conditions (*13*).

To address this limitation, we integrated an algorithm that accounts for the adverse impacts of flooding on crops to refine the initial outcomes of GGCMI3 simulations, with flooding conditions identified from global daily inundation simulations (see Materials and Methods for details). The response of the adjusted GGCMI3 crop yields to water availability anomalies is depicted by blue lines in Fig. 1. This adjustment substantially reduced crop yields under extreme wet conditions and substantially improved the model performance. Each individual model also benefited from this adjustment (figs. S6 to S8), although the magnitude of improvement varied slightly across models. Spatially, the most affected areas for all three crops were the Midwestern states, including Iowa, Minnesota, Nebraska, and North Dakota (fig. S9, A to C). For wheat, notable impacts also appeared in California (west) and North Carolina and Virginia (east). In these regions, the original simulations predominantly predicted a positive yield change, whereas the adjusted simulations successfully captured the spatial patterns of yield reductions under extreme wet conditions (fig. S9, G to I). Overall, these findings indicate that our proposed parametrization mostly reproduced the observed impact of flooding on crops in the United States, which could serve as a valuable tool for assessing and predicting flood-induced crop losses.

## Estimation and validation of flood-induced agricultural losses

Flood-induced crop damage incurs substantial economic losses for farmers and the agricultural sector. On the basis of the estimated reduction in crop production, the associated economic losses were calculated using crop prices (see Materials and Methods for details). However, it should be noted that flooding may affect agriculture and the economy in multiple ways. Because the FAO provides country-level crop price data only from 1991 onward, our estimates of agricultural losses also begin in that year. We compared these estimates with flood-related indemnity payments reported by the USDA Risk Management Agency (USDA-RAM) over the same period. As illustrated in Fig. 2 (A to C), the time series of indemnities and estimated losses across the United States exhibited a consistently strong correlation. The rank-order correlations between the two datasets were 0.62 ($P < 0.01$), 0.47 ($P < 0.05$), and 0.34 ($P = 0.11$) for maize, soybean, and wheat, respectively. To further evaluate performance, we introduced consistency indices ($CI_5$ and $CI_{10}$), which measure the proportion of years ranked among the top 5 (or top 10) in reported losses that were also ranked among the top 5 (or top 10) in estimated losses. These indices provide a more targeted assessment of the method's ability to capture high-impact events. The CI values indicated satisfactory agreement, with about three-fifths of major loss years successfully identified. Spatially, states with high estimated losses closely corresponded to those with high reported indemnities across all three crops, with significant positive correlations (Fig. 2, D to I). Together, these results suggest that our methodology effectively captured the magnitude and distribution of substantial crop damage caused by flooding, both temporally and spatially.

In addition, we found that the adjusted yield simulations provided a more realistic representation of the relative magnitude of drought- and flood-induced losses. Reported indemnities show that average annual drought-induced losses were generally higher than flood-induced losses, with a ratio of about 1.5 to 2 across the three crops (Fig. 3A). By contrast, loss estimates derived from the original yield simulations suggested that extreme dry condition losses ($loss^{ED}$) were vastly greater than extreme wet condition losses ($loss^{EW}$), with ratios exceeding 20 for maize and soybean. After applying the flood-impact adjustment, the ratio of $loss^{ED}$ to $loss^{EW}$ aligned much more closely with indemnity records. Beyond national totals, we also compared the proportions of states falling into different ratio categories (Fig. 3B). On the basis of reported indemnities, 26, 19, and 62% of states experienced higher flood- than drought-induced

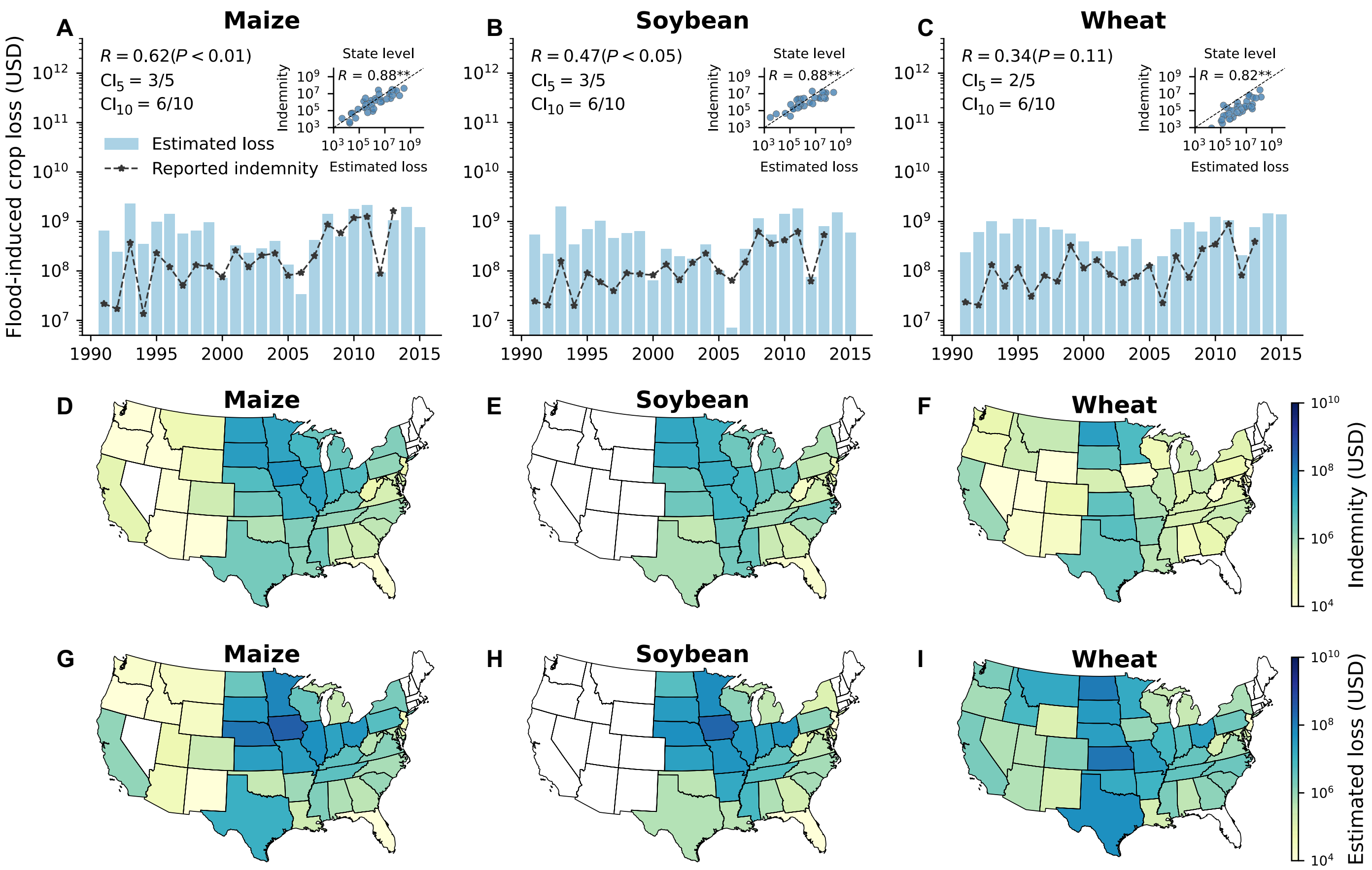


**Fig. 2. Comparison of reported flood-induced indemnities and estimated crop losses in the continental United States.** (**A** to **C**) Time series of annual reported indemnities due to excessive rainfall and flooding (from USDA-RMA) and estimated flood-induced losses for maize (A), soybean (B), and wheat (C) during 1991 to 2015. Spearman's rank correlation coefficients (*R*) and their significance levels are shown. The consistency indices ($CI_5$ and $CI_{10}$) represent the proportion of years in which the top 5 (or top 10) years of reported indemnities also appear among the top 5 (or top 10) years of estimated losses. The insets display scatterplots of state-level reported indemnities versus estimated losses, with corresponding *R* values and significance levels (**$P < 0.01$, two-sided Spearman correlation test). (**D** to **F**) Spatial distribution of average annual flood-induced indemnities for maize, soybean, and wheat across individual states during 1991 to 2015. (**G** to **I**) Spatial distribution of the corresponding estimated flood-induced crop losses for maize, soybean, and wheat.

losses for maize, soybean, and wheat, respectively. The original yield simulations severely underestimated these proportions (<10%), whereas the adjusted yield simulations reproduced them much more accurately.

We further extended this method to the global scale, applying it to adjust the original yield simulations and to estimate flood-induced crop losses worldwide. However, validating flood-induced crop yield reductions and their associated economic losses on a global scale is challenging due to limited data availability. To the best of our knowledge, the most comprehensive and reliable datasets for flood-induced losses (covering all sectors, not just agriculture) are provided by the EM-DAT. Therefore, we compared our estimates of flood-induced crop losses with the annual economic losses from flooding at the national level as reported by the EM-DAT. As shown in fig. S10, the global total losses of maize, soybean, and wheat exhibited good temporal agreement with EM-DAT flood-related damages ($R = 0.62$, $CI_5 = 3/5$, and $CI_{10} = 6/10$). Among countries with available data, about 71% captured at least two of the top 5 loss years ($CI_5 \geq 2/5$), and 34% captured at least three ($CI_5 \geq 3/5$). These results indicate that our approach generally identifies major flood-induced crop losses at the global scale. Nevertheless, these estimates should be interpreted with caution as the adjustment method was developed using US crop yield data and has not yet been independently validated with yield observations from other regions; moreover, the EM-DAT reports total damages across all sectors rather than agricultural losses exclusively.

## Projected flood-induced agricultural losses under future climate change

Using the same methodology, we adjusted the projected crop yield responses to future climate change provided by GGCMI Phase 3b (see Materials and Methods for details). In the United States, the original yield projections suggested minimal agricultural losses under extreme wet conditions, with $loss^{ED}$ exceeding $loss^{EW}$ by more than twofold in nearly all states. However, as clearly demonstrated in Fig. 1, this prediction is biased because the original crop models failed to adequately represent the flood impacts on crop yields. After incorporating the crop flooding stress adjustment, the projected average annual $loss^{EW}$ during 2015 to 2100 under SSP585 would reach ~$287 million, $234 million, and $212 million for maize, soybean,

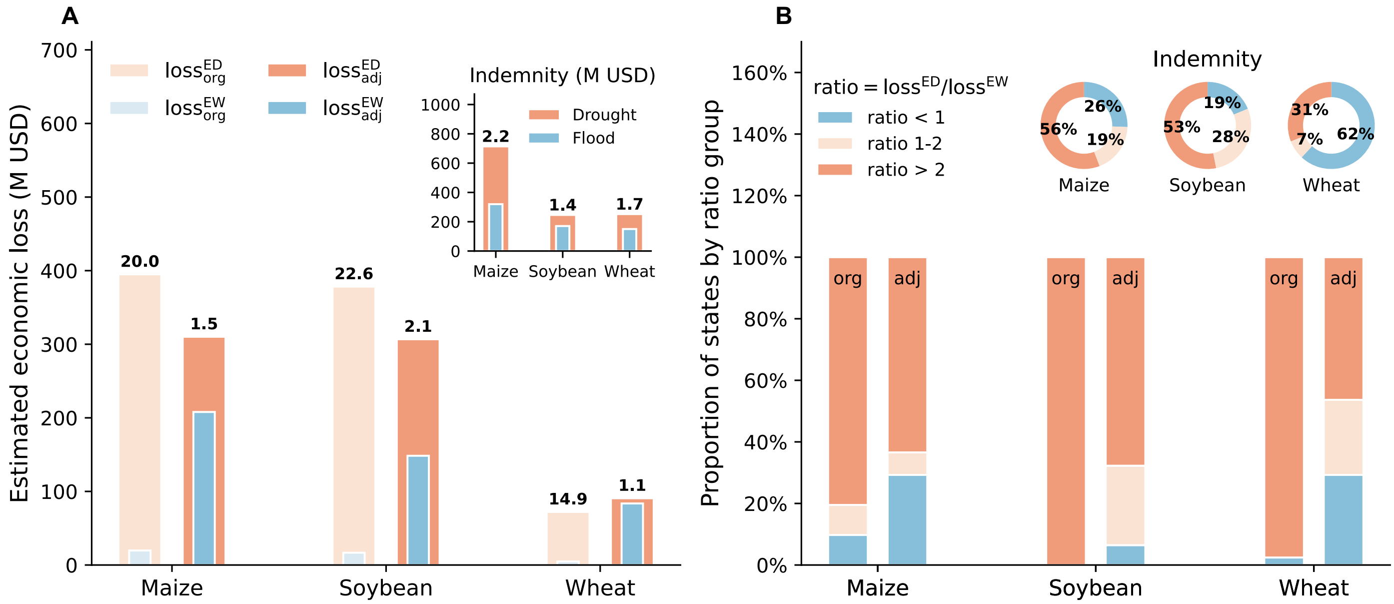


**Fig. 3. Comparison of crop losses under extreme dry and wet conditions in the continental United States.** (**A**) Mean annual crop losses in extreme dry conditions (ED) and extreme wet conditions (EW) for maize, soybean, and wheat, based on original (org) and adjusted (adj) crop simulations. Numbers above the bars denote the ratio of losses in ED relative to EW. The inset shows mean annual drought- and flood-induced indemnity amounts for the three crops. (**B**) Ratios of estimated losses in ED to those in EW, expressed as the proportion of states falling into different ratio ranges for the three crops, based on original and adjusted crop simulations. The inset shows analogous results for the ratio of drought- to flood-induced indemnities.

and wheat, respectively. Moreover, $loss^{EW}$ is anticipated to surpass $loss^{ED}$ in about 40, 27, and 55% of states for these crops (Fig. 4, A to C). High-risk states include Illinois, Indiana, Iowa, Kansas, Minnesota, Mississippi, Missouri, and Nebraska, a distribution that closely aligns with states historically reporting high flood-induced indemnities (Fig. 2).

Temporally, flood risks are expected to intensify under high-emission scenarios, with increasing flood depths (Fig. 4, D to F). The $loss^{EW}$ for soybean and wheat are projected to generally rise with flood depths under SSP585, whereas maize shows a slight decline in $loss^{EW}$. As a C4 crop, maize gains limited photosynthetic benefit from elevated $CO_2$, and higher temperatures tend to suppress growth, reducing yields. Consequently, even under comparable or slightly increased flood risks, maize losses tend to decrease. We also examined the sensitivity of future crop loss estimates to pricing assumptions (see text S4). Using a dynamic crop price approach, which accounts for price increases under reduced yields (fig. S20), produces higher absolute loss estimates, but the main conclusions—including the relative differences between losses under extreme dry and extreme wet conditions, as well as the projected trends in $loss^{EW}$—remain broadly consistent (fig. S21).

Under the low-emission SSP126 scenario, projected crop losses differ from those under SSP585, with soybean and wheat losses slightly lower and maize losses slightly higher (fig. S11). This pattern again reflects maize's distinct response to elevated $CO_2$ compared with soybean and wheat. Notably, the upward trends in flood risks and associated crop losses are less pronounced under SSP126 (fig. S11, D to F), with projected wheat losses shifting from a significant increase under SSP585 to a slight decrease under SSP126. These results highlight the potential benefits of emission reductions in mitigating future food risks.

Extending the projections to the global scale, the adjusted simulations once again reveal that, in contrast to the original projections, flood-induced crop losses are likely to be comparable to or even exceed drought-induced losses across many regions under the future climate scenario (fig. S14). We further identified the countries with the highest projected crop losses and their associated economic losses. These countries correspond to those with extensive crop areas and a history of high flood risk, including the United States, China, Brazil, India, and Mexico (Fig. 5, A to C). However, when considering economic status and population size, these nations are not the most vulnerable (Fig. 5, D to I). In low-income developing countries, where household food supplies and economic development heavily depend on specific crops, flood-induced losses have a disproportionately large impact. For instance, wheat losses in some Central Asian countries could reach ~1.0 per mil (‰) of gross domestic product (GDP), compared with a global average of ~0.04‰ (Fig. 5F). In South America, per capita soybean losses in countries such as Argentina, Paraguay, and Bolivia are projected to be 20 to 30 times higher than the global average (Fig. 5H). Similarly, maize losses in many African nations could pose notable challenges to already fragile local economies (Fig. 5D). Although these projections inevitably involve uncertainties, they provide valuable insights into spatial disparities in agricultural impacts of flooding and highlight vulnerable regions where targeted adaptation and risk management efforts are urgently needed.

## DISCUSSION

Global warming is expected to intensify rainfall extremes, increasing both drought and flood risks (*32*). Although current global crop models capture yield losses under drought, they largely fail to represent

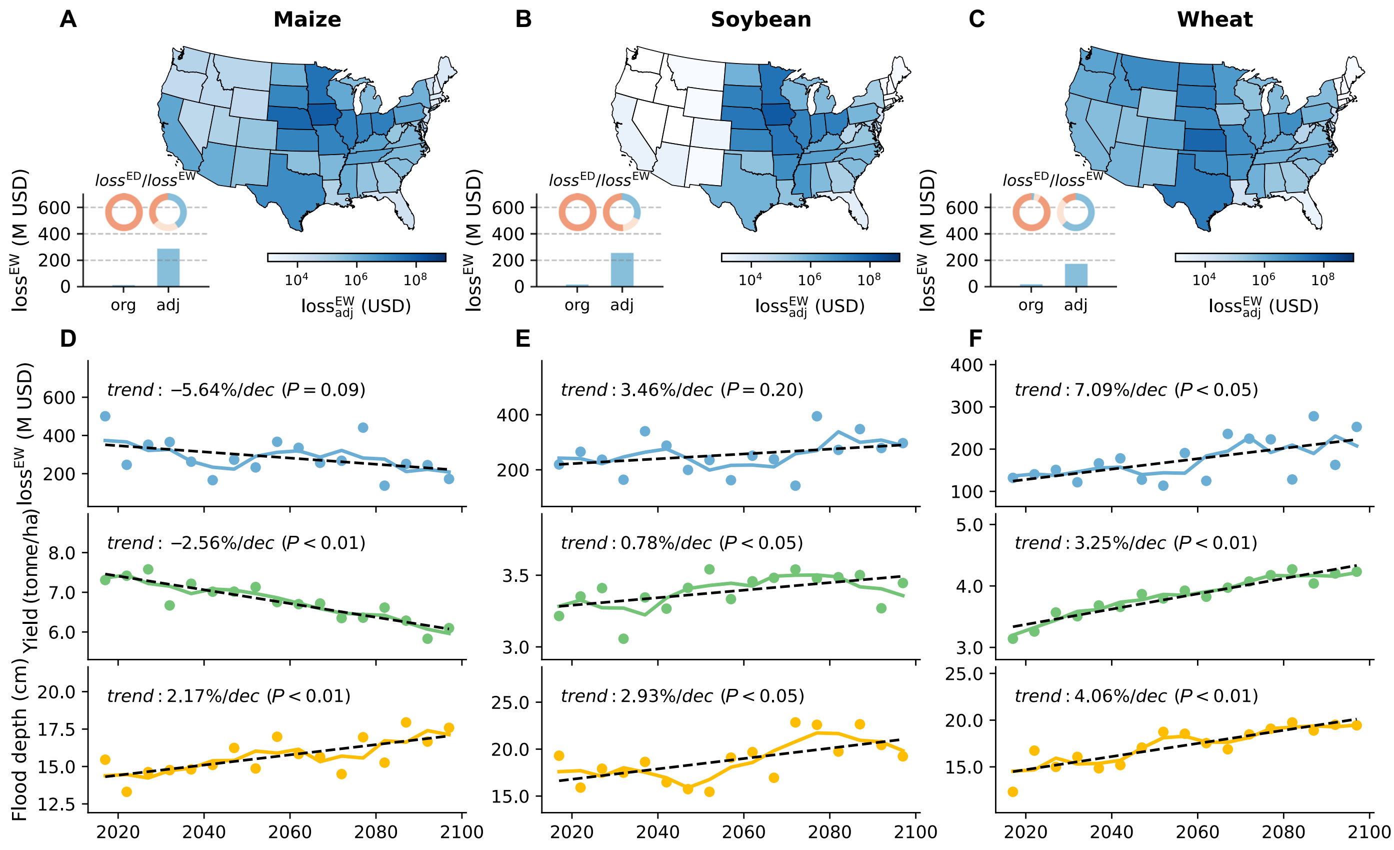


**Fig. 4. Crop losses under extreme wet conditions in the United States under the SSP585 scenario based on the static price assumption.** (**A** to **C**) State-level annual crop losses under extreme wet conditions ($loss^{EW}_{adj}$) for maize, soybean, and wheat, respectively, averaged over 2015 to 2100. The inset compares national annual losses under extreme wet conditions based on original and adjusted yield projections ($loss^{EW}_{org}$ versus $loss^{EW}_{adj}$). The ring chart shows the proportion of states in different ratio categories, where the ratio is defined as $loss^{ED}/loss^{EW}$, calculated from original and adjusted projections. As in Fig. 3, blue indicates a ratio of <1, light pink indicates 1 to 2, and pink indicates >2. (**D**) Time series of total crop losses, yields, and average flood depth for maize in the United States from 2015 to 2100, with the black dashed line indicating the ordinary least-squares regression trend; significance is assessed using a two-tailed Student's *t* test. The dots denote 5-year averages (centered on the given year), and the solid curves represent the moving averages. (**E** and **F**) Same as (D) but for soybean and wheat. dec, decade.

flood-induced damages, limiting reliable projections of future agricultural risks. To address this gap, we developed an innovative framework that quantifies crop flooding stress by integrating state-of-the-art global crop yield and flood simulations. Conceptually, the framework uses a top-down strategy that couples two physics-based models—a crop model and a floodplain model—through a crop flooding stress algorithm. The algorithm represents the flood impacts on crops using a monotonically increasing convex curve with an upper asymptote (fig. S4). Two parameters, linked to soil properties (drainage capacity and water-holding capacity) and crop type, shape this curve. Unlike conventional bottom-up modeling approaches (*12*, *28*–*30*), which simulate specific physiological processes of crop growth—such as photosynthesis, root development, phenology, and nutrient uptake, our method provides a generalized representation that avoids the complexity and uncertainties associated with numerous process-specific parameters. This approach, although currently applied only to maize, soybean, and wheat due to data limitations, is simple, efficient, and readily extendable to other crops and production systems.

Validation demonstrates that the adjusted simulations align well with observed yield responses to flooding (Fig. 1) and provide reliable estimates of flood-induced economic losses at both regional and global scales (Figs. 2 to 3 and fig. S10). When applied to future climate scenarios, the framework—unlike projections based on the original yield estimates suggesting very limited impacts from flooding—indicates that flood-induced losses could be comparable to or even exceed drought-induced losses in many regions (Fig. 4 and fig. S14). Although multiple models introduce considerable uncertainty (crop models, in particular, are likely a major source of variability compared to climate and hydrological models; figs. S12 and S13), these findings underscore the importance of giving flood mitigation equal priority alongside drought management to address potential food crises under future climate change.

Despite these improvements, the flooding stress adjustment implemented here remains a simplified approximation. Crop yield reductions from excessive water can arise through multiple pathways, including prolonged soil saturation, impaired root respiration, reduced solar radiation, nutrient leaching, and heightened pest and disease pressures (*12*, *13*, *28*, *33*). The severity of these impacts also depends strongly on the timing of flood events as crop vulnerability to flooding varies across different growth stages (*8*, *9*, *34*). Moreover, future changes in temperature, precipitation, $CO_2$ concentrations, and agricultural technologies (e.g., hybrid cultivars and improved

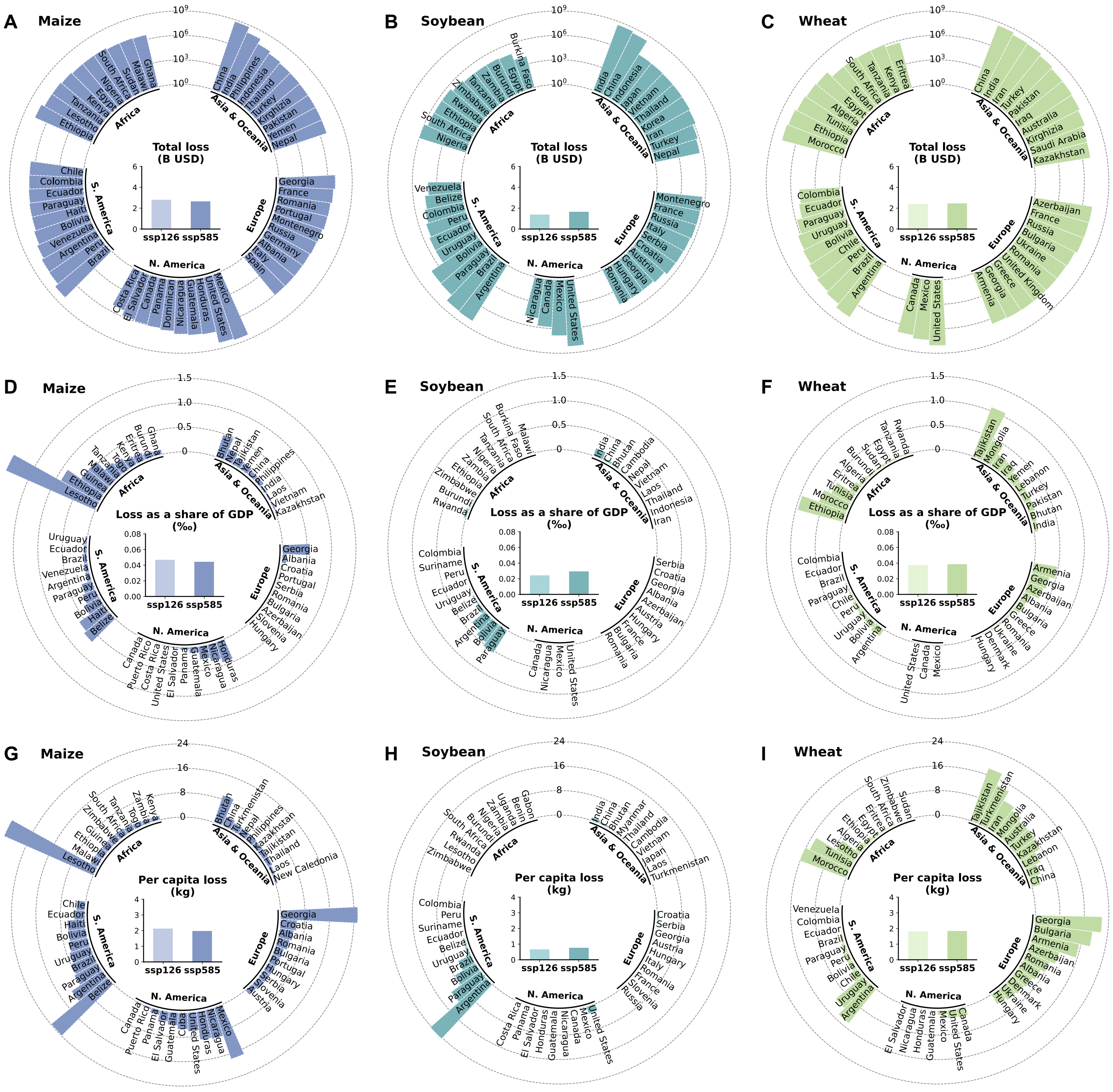


**Fig. 5. Projected crop losses under extreme wet conditions in future climate scenarios.** (**A** to **C**) Projected losses of maize, soybean, and wheat under the SSP585 scenario for the top 10 most affected countries on each continent (outer bars). Middle bars show the corresponding global losses under both SSP126 and SSP585 scenarios. (**D** to **F**) Same as (A to C) but expressed as a share of national GDP. (**G** to **I**) Same as (A to C) but expressed as per capita production losses.

soil and nutrient management) may have interactive effects on crops (*35–37*) that are difficult to capture within our current framework. Thus, the method should be regarded as a pragmatic empirical solution, rather than a substitute for fully mechanistic models. It represents a useful interim step reflecting current model limitations. Advancing global crop modeling will require tighter coupling of hydrological and agronomic processes, incorporation of physiological crop responses to inundation, and coordinated multimodel experiments. As these developments mature, empirical adjustments like ours may be refined or replaced by comprehensive process-based approaches.

Another limitation lies in the economic assumptions underpinning our loss estimates. First, our estimation of future crop prices was simplified, relying on two approaches: a static assumption based on historical averages and a projection derived from historical yield-price relationships. However, crop prices are also influenced by broader economic factors such as inflation, policies, and market dynamics (*38*). Future studies should address this limitation by coupling crop models with economic frameworks that simulate market responses, trade, and policy effects to provide more comprehensive projections of economic shocks. Second, our loss estimates assume static future farm management and harvested areas. In practice, farmers may adopt adaptive strategies to mitigate flood risks, including changing planting dates, switching crop varieties, and implementing engineering measures to reduce flood exposure. Likewise, future harvested areas may shift in response to socioeconomic drivers such as land value, global demand, and policy incentives (*39*, *40*). Because total production depends on both yield and harvested area, these changes could either buffer or amplify climate-induced impacts. Capturing these interactions would require coupling crop models with integrated assessment models or other socioeconomic frameworks capable of representing dynamic land-use and management decisions. Although such integration is beyond the scope of this study, we acknowledge that omitting adaptive behavior and land-use dynamics introduces notable uncertainty into our crop loss projections. Therefore, our results should be interpreted as scenario-based assessments that reflect potential climate risks under static management assumptions. Last, our analysis focuses on direct local impacts, neglecting secondary effects transmitted through global trade. For example, subsequent increases in food prices and potential export restrictions could further exacerbate food security challenges, particularly in import-dependent regions (*41*, *42*). Overall, future flood-induced agricultural losses depend not only on climate trajectories but also on adaptation measures and feedbacks operating across multiple levels—from farmers to institutions and policy systems.

In summary, this study underscores the substantial and escalating risks of flood-induced crop losses under high-emission scenarios, although outcomes vary across crops and regions. The estimations provide a scientific basis for strategic adaptation, including shifting cultivation from high-risk to low-risk zones and strengthening flood prevention and management. Effective measures may include afforestation, crop variety improvements, restoration of riparian vegetation, and engineering interventions such as dredging, straightening, stabilization, levees, and enhanced drainage. By identifying hotspots of vulnerability and quantifying potential losses, our findings contribute to prioritizing disaster risk reduction and adaptation strategies, offering critical insights for protecting both agricultural systems and the populations that depend on them.

## MATERIALS AND METHODS

### Crop yield and insurance data in the United States

County-level yield and harvest area data from 1980 to 2015 were obtained from the USDA National Agricultural Statistics Service (USDA NASS; https://quickstats.nass.usda.gov/). The NASS dataset is compiled from multiple sources, primarily extensive surveys conducted during the production year (including area-frame surveys, stratified sampling of farms, and farmer interviews) (*43*). Recognized as the highest quality crop production data in the United States, this dataset has been extensively used in climate and agriculture studies (*21*, *44*). According to these data, maize, soybean, and wheat are the most widely distributed and high-production crops in the US. Given the necessity for ample observational data for calibration, this study focuses on these three crops. County-level crop insurance data for the same period were obtained from the USDA-RMA. These data include details on the "Cause of Loss" (https://legacy.rma.usda.gov/data/cause.html) and "Summary of Business" (https://www.rma.usda.gov/tools-reports/summary-of-business), which specify the causes of loss reported by farmers (e.g., drought, heat, and excessive rainfall), as well as the indemnity and premium amounts for various causes of loss (fig. S1). Daily precipitation data from 1980 to 2015, with a 4-km spatial resolution, were obtained from PRISM (https://prism.oregonstate.edu/) (*45*).

### Global crop simulations

This study uses crop model simulations from GGCMI3, which is part of the Agricultural Model Intercomparison and Improvement Project (AgMIP) and contributes to the agricultural sector of the Inter-Sectoral Impact Model Intercomparison Project (ISIMIP). GGCMI Phase 3 consists of two components: Phase 3a, in which all crop models are driven by historical climate reanalysis data (GSWP3-W5E5), and Phase 3b, which uses bias-adjusted and downscaled CMIP6 climate projections harmonized within ISIMIP3b. All simulations are conducted at a 0.5° global grid resolution. A detailed description of the GGCMI Phase 3 crop modeling protocol is available in Jägermeyr *et al.* (*17*). A brief overview is summarized below.

Model harmonization in GGCMI3 mainly involves standardized inputs for crop calendar, fertilizer applications, and soil characteristics. Additional protocol elements are recommended but not mandatory as not all models can accommodate every feature. The crop calendar, provided by Jägermeyr *et al.* (*17*), specifies planting and maturity dates for each crop and grid cell, separately for rainfed and irrigated systems. Growing season inputs are held constant over time to avoid confounding trends. Each model calculates the reference heat units required for physiological maturity by averaging annual heat sums across growing seasons from 1979 to 2010. Fertilizer management includes mineral fertilizer inputs ($NH_4NO_3$), which are crop specific and derived from the LUH2 dataset, and manure application inputs (C:N ratio, 14.5) that are grid cell specific but constant across crops. Fertilizer is applied following a simple schedule: 20% at sowing and 80% when 25% of the required heat units have accumulated. All other nutrients are assumed nonlimiting. Atmospheric nitrogen deposition, separated into $NH_x$ and $NO_y$ components, is fixed at 2015 levels (*46*). Soil input data are primarily obtained from the Harmonized World Soil Database (HWSD), aggregated to 0.5° resolution to be cropland specific. Some models use alternative datasets (e.g., the Global Soil Dataset for Earth System Modelling) due to difficulties in retrieving all soil parameters from the HWSD (*47*, *48*). All crops are simulated under both rainfed and fully irrigated conditions. Irrigation is implemented by resetting soil moisture daily to field capacity without water limitations. Simulations are independent of present-day cropland distribution; in post-processing, cropland extent and irrigated fractions are imposed using the MIRCA2000 dataset (Global Data Set of Monthly Irrigated and Rainfed Crop Areas around the Year 2000) (*49*).

For the historical analysis, we used GGCMI Phase 3a outputs driven by the GSWP3-W5E5 climate dataset. Simulations were conducted with and without irrigation under default settings (i.e., standard assumptions for crop calendars, fertilizer inputs, and soil parameters) and static socioeconomic inputs (i.e., socioeconomic factors and farm management practices fixed at 2015 levels). We focused on three major crops—maize, soybean, and wheat—given their broad cultivation in the United States and the availability of extensive yield observations. Crop models that provided yield simulations for all three crops were selected, including ACEA, CROVER, EPIC-IIASA, ISAM, LDNDC, LPJmL, pDSSAT, PEPIC, PROMET, and SIMPLACE-LINTUL5.

For the future projections, we used GGCMI Phase 3b outputs, which contribute to CMIP6 impact assessments in coordination with ISIMIP Phase 3b, where GGCMI represents the agriculture sector. All simulations assumed fixed year-2015 direct human influences and used default settings. Climate inputs were derived from bias-adjusted and downscaled CMIP6 model outputs, processed within the ISIMIP framework to provide daily data on a 0.5° × 0.5° global grid. Bias adjustment was conducted using a quantile-mapping approach based on the observational W5E5 v1.0 dataset. Future climate projections considered five CMIP6 models—GFDL-ESM4, UKESM1-0-LL, MPI-ESM1-2-HR, IPSL-CM6A-LR, and MRI-ESM2-0—which together span a broad range of equilibrium climate sensitivity, under two climate change scenarios: a high-emission pathway (SSP585) and a low-emission pathway (SSP126).

### Yield response to extreme climates

We used the yield percentage change ($\Delta Y_i$), which was calculated as the difference between the actual yield ($Y_i$) and the trend yield ($YT_i$) for a specific year $i$ divided by the trend yield ($YT_i$), to assess the impact of extreme climates on crop yield

$$\Delta Y_i = \left(Y_i - YT_i\right) / YT_i \times 100\% \tag{1}$$

The trend yield was estimated by fitting a linear trend to the annual yield time series over the study period using least-squares regression. The resulting temporal trend generally reflects improvements driven by technological advances, enhanced management practices, and long-term climate influences such as rising $CO_2$ concentrations. Deviations from this trend can be attributed to external shocks, including extreme climate events, plant diseases, violent conflicts, or epidemics. As extreme climate events occur more frequently than other disruptive factors, this method is commonly used to assess the impacts of extreme climatic conditions on yield variability (*11*).

The extreme climates, referring to the extremes in water availability for crops in this study (either dry or wet conditions), were assessed using standardized anomalies, commonly known as *z*-scores, of growing-season precipitation. These standardized anomalies were calculated by quantifying the deviation of annual growing-season precipitation from its climatological value and subsequently normalizing it by the SD (σ). Extreme dry conditions were defined as precipitation anomalies below −2σ, and extreme wet conditions were defined as anomalies exceeding +2σ.

On the basis of the yield percentage changes and their corresponding precipitation anomalies for each county-year sample, we derived the crop yield response to extreme climates (Fig. 1) by calculating the average yield percentage change within individual precipitation anomaly bins (at intervals of 0.5σ). Within each bin, the yield percentage change was determined as the weighted average, considering all county-year samples falling within that particular bin, with the weighting factor being the harvest area. For individual counties, calculating the average impact of extreme climates involves determining the weighted average yield percentage change over the years identified as extreme, again using the harvest area as the weighting factor.

To compare the outcomes of crop model simulations with observations, we aggregated the observed yield percentage change and harvest area for each county to a 0.5° grid box, following the method outlined by Li *et al.* (*13*). If a county's center falls within a 0.5° grid box, we assigned the county and its corresponding crop yield and harvest area to that specific grid box. In cases where a grid box contains multiple counties, we calculated the average values of crop yield using an area-weighted approach. The harvest area was aggregated for that grid box. Subsequently, we computed the responses of observed and simulated crop yield to extreme climates using the area-weighted aggregation method described above.

### Global flooding simulations

We applied the Catchment-based Macro-scale Floodplain model (CaMa-Flood) to simulate global river-floodplain hydrodynamics at a daily scale. CaMa-Flood discretizes the entire river networks into irregular unit-catchments with the subgrid topographic parameters for the river channel and floodplains. It uses a diagnostic scheme at the unit-catchment scale to approximate the complex processes of floodplain inundation. To optimize the prognostic computation of water storage, it implemented the local inertial equation and an adaptive time-step scheme. This approach offers high computational efficiency, which is advantageous for global-scale implementations. The river-floodplain parameterizations for the model were derived from the MERIT Hydro (Multi-Error-Removed Improved-Terrain) dataset, which is based on the MERIT DEM and multiple inland water body datasets (*50*, *51*). A comprehensive description of the model's physics, parameterization methods, and sensitivities to input parameters can be found in the previous literature (*52*–*54*). In our study, CaMa-Flood was driven by global hourly runoff data spanning the period from 1981 to 2010, obtained from the ERA5-Land hourly dataset (*55*), with river topography maps at a spatial resolution of 0.25°.

CaMa-Flood has been widely validated and proven effective in simulating river flow processes and flooding dynamics (*15*, *56*). Here, we validated the simulated global historical flood dynamics by comparing them with satellite-based water surface observations. Global Inundation Extent from Multi-Satellites (GIEMS) data (*57*) serve as the most commonly referenced satellite inundation maps for validating model performance across extensive areas and over long periods, available monthly from 1993 to 2007. Figure S3 illustrates the global distribution of simulated and satellite-based average annual maximum inundation fractions. The simulation accurately captured regions where the satellite-based inundation fraction exceeded 0.1 with an accuracy of 97%. Although 28% of grids with a simulated inundation fraction greater than 0.1 were not observed in the remote sensing data, many of these corresponded to lakes, such as the Great Lakes in the United States (fig. S3B). In addition, there is strong temporal consistency between the simulations and the satellite-based dataset, with positive correlations observed in approximately 75% of the grids.

### An empirical adjustment for flooding stress in global crop simulations

Given the lack of explicit flood response mechanisms in most global process-based crop models, we implemented an empirical adjustment to approximate the impacts of flooding on crop yields. Specifically, we adjusted the simulated yields using the following equation

$$Y_{adj} = Y_{org} \times \left(1 - f_{adj}\right) \tag{2}$$

where $Y_{org}$ denotes the original crop yields simulated by global crop models participating in GGCMI3 (tonne $ha^{-1}$ $year^{-1}$), $Y_{adj}$ denotes the adjusted crop yields, and $f_{adj}$ is a dimensionless coefficient ranging from 0 to 1 that represents the fractional yield loss due to flooding.

Flooding is quantified in terms of floodplain water depth, which can be simulated using CaMa-Flood. When an area experiences continuous flooding for 5 consecutive days, the crops are considered to be affected by floods. In this study, we used the annual maximum value of the minimum floodplain water depth over 5 consecutive days ($fd_{5d-max}$; cm) during the crop growing period (from planting day to maturity day) to represent the magnitude of floods that affect crop yields in a given year. With fixed crop type and location, $f_{adj}$ exhibits the following characteristics: (i) $f_{adj}$ ranges from 0 to 1, (ii) a larger value of $fd_{5d-max}$ corresponds to a larger $f_{adj}$, and (iii) as $fd_{5d-max}$ rises, the increase in $f_{adj}$ due to a one-unit increase in $fd_{5d-max}$ shows a marginally decreasing pattern (i.e., increasing the water depth merely causes a smaller increase in $f_{adj}$ when the water depth is already high). Therefore, we used the following equation to quantify the relationship between $fd_{5d-max}$ and $f_{adj}$ (fig. S4)

$$f_{adj} = \frac{fd_{5d-max}}{\left(1 + fd_{5d-max}{}^{f_v}\right)^{1/f_v}} \quad (3)$$

where $f_v$ is a parameter that determines the shape of the $fd_{5d-max} \sim f_{adj}$ curve. As $f_v$ increases, the corresponding $f_{adj}$ for the same $fd_{5d-max}$ rises. Thus, this parameter indicates the vulnerability of the crop and/or region to flooding, with a higher $f_v$ representing higher vulnerability.

The vulnerability parameter ($f_v$) can be determined by two key factors: the tolerance of crops to waterlogging ($v_{crop}$) and the soil hydraulic properties ($v_{soil}$), as indicated in Eq. 4. Regions with higher soil saturated hydraulic conductivity (*ks*, representing drainage capacity) and larger root zone soil water storage capacity (*ws*, representing water-holding capacity) are less likely to experience detrimental waterlogged conditions for crops. Therefore, we used Eq. 5 to calculate the parameter $v_{soil}$ that represents flooding vulnerability related to soil hydraulic properties. In this equation, we standardized *ks* and *ws* by dividing them by their respective global mean values to obtain dimensionless parameters $ks_{norm}$ and $ws_{norm}$ (fig. S2). The global *ks* and *ws* data were obtained from a global dataset of soil hydraulic parameters provided by Dai *et al.* (*58*) and a Global Soil Texture and Derived Water-Holding Capacities dataset provided by Webb *et al.* (*59*), respectively

$$f_v = v_{crop} \times v_{soil} \quad (4)$$

$$v_{soil} = 1/\left(ks_{norm} \times ws_{norm}\right) \quad (5)$$

The parameter representing the vulnerability of crops to waterlogging ($v_{crop}$) was estimated through calibration. Specifically, we calculated $Y_{adj}$ on the basis of an assumed $v_{crop}$ value and then compared the response curve of $Y_{adj}$ to extreme climates with that of $Y_{obs}$ to extreme climates. The optimal $v_{crop}$ was identified as the value that minimized the bias between the two curves. We further conducted a cross-validation analysis to evaluate the robustness of the calibrated parameter (see text S2 for details).

### Crop loss estimation and validation

Crop loss due to flooding, measured in US dollars (USD), was estimated using the following equation

$$loss_{i,c} = \min\left(0,\ Y_{adj}^{i,c} - Y_{org}^{i,c}\right) \times A_c \times V_{i,c} \quad (6)$$

$$V_{i,c} = P_{i,c} \times \alpha \quad (7)$$

In this equation, $Y_{org}^{i,c}$ and $Y_{adj}^{i,c}$ represent the original and adjusted crop yield simulations, where the subscripts *i* and *c* denote the indices for the year and grid/country, respectively. *A* is the harvested area (in hectares, ha), obtained from global gridded harvest area data at a 0.5° resolution (*49*). *V* denotes the loss or indemnity value per unit crop weight (USD tonne$^{-1}$). Because detailed indemnity policy data are not globally available, we approximated *V* as the product of crop market price (*P*) and an indemnity coefficient (α). Details on the specifications of *P* and α, as well as their influence on loss estimates, are provided in text S3. The loss estimates presented in the main text are based on the 5-year average crop price and a stepwise indemnity coefficient that increases progressively with yield loss severity. Country-specific crop prices from 1991 to 2015 were obtained from the FAO statistical database (www.fao.org/faostat/en/#data/PP). When price data were not available for specific countries or years, we substituted the median price across all other countries for that year.

In the United States, we compared the estimated flood-induced crop losses with the indemnity amounts reported by the USDA-RMA on both spatial and temporal scales for individual crops. Globally, we contrasted the estimated crop losses due to floods against the annual economic damages caused by flooding at the country level, as documented by the EM-DAT (*10*). Although the EM-DAT, being a country-level, self-reported database of extreme events, may introduce biases due to varying standards among countries and other factors, it is still recognized as one of the most detailed and reliable datasets for disaster losses globally, extensively used across multiple disciplines (*16*, *60*).

To compare crop losses under extreme dry and wet conditions, we applied a similar approach. Crop losses under extreme dry conditions were estimated using

$$loss_{ED} = \min\left(0, Y_{ED} - YT_{ED}\right) \times A \times V \quad (8)$$

Here, the subscript ED denotes the extreme dry conditions, $Y_{ED}$ represents the crop yield under extreme dry conditions, and $YT_{ED}$ is the corresponding trend yield. *A* and *V* are defined as in Eqs. 6 and 7. It should be noted that extreme dry and wet conditions were identified at the grid cell level. Their impacts on crop yield were likewise estimated at the grid cell scale and subsequently aggregated to the state or national level, rather than being calculated directly at those larger scales.

### Crop loss projection under future climate scenarios

To adjust crop yield simulations in GGCMI Phase 3b and project future crop losses, we first performed flood simulations under future climate scenarios. Global runoff projections from six hydrological models—classic, h08, jules-w2, miroc-integ-land, watergap2-2e, and web-dhm-sg—were used within the ISIMIP3b framework. The climate inputs for these hydrological models were the same bias-adjusted and downscaled CMIP6 projections used for the crop models. The resulting runoff data were subsequently input into CaMa-Flood to simulate global river-floodplain hydrodynamics under future climate conditions.

Next, we applied the same methodology used for historical periods to adjust future crop yield predictions based on the flooding simulations, thereby estimating future crop losses. For historical periods, losses were estimated using reported crop prices. For future analyses, two crop price schemes were considered: (i) a static price, based on the historical average, and (ii) a dynamic price, derived from the historical yield-price relationship. Detailed information is provided in text S4. The results presented in the main text are based on the static price approach.

To further contextualize the economic impact, we used a global gridded dataset of GDP from 1991 to 2015 to calculate crop losses as a share of GDP for individual countries. In addition, a global gridded population dataset at 5-year intervals for 2020 to 2100 under different emission scenarios (*61*) was used to estimate per capita losses.

## Supplementary Materials

**This PDF file includes:**
Figs. S1 to S21
Supplementary Text S1 to S4
Table S1

## REFERENCES


1. P. Wallemacq, R. House, "Economic Losses, Poverty & Disasters: 1998-2017" (Centre for Research on the Epidemiology of Disasters and United Nations Office for Disaster Risk Reduction, 2018).
2. Centre for Research on the Epidemiology of Disasters (CRED), "2022 Disasters in Numbers" (CRED, 2023).
3. B. Tellman, J. A. Sullivan, C. Kuhn, A. J. Kettner, C. S. Doyle, G. R. Brakenridge, T. A. Erickson, D. A. Slayback, Satellite imaging reveals increased proportion of population exposed to floods. *Nature* **596**, 80–86 (2021).
4. H. Webber, G. Lischeid, M. Sommer, R. Finger, C. Nendel, T. Gaiser, F. Ewert, No perfect storm for crop yield failure in Germany. *Environ. Res. Lett.* **15**, 104012 (2020).
5. Food and Agriculture Organization of the United Nations (FAO), "The Impact of Disasters and Crises on Agriculture and Food Security" (FAO, 2021).
6. M. Shirzaei, M. Khoshmanesh, C. Ojha, S. Werth, H. Kerner, G. Carlson, S. F. Sherpa, G. Zhai, J.-C. Lee, Persistent impact of spring floods on crop loss in U.S. Midwest. *Weather. Clim. Extrem.* **34**, 100392 (2021).
7. R. E. Shaw, W. S. Meyer, A. McNeill, S. D. Tyerman, Waterlogging in Australian agricultural landscapes: A review of plant responses and crop models. *Crop Pasture Sci.* **64**, 549–562 (2013).
8. L. Tian, Y. Zhang, P. Chen, F. Zhang, J. Li, F. Yan, Y. Dong, B. Feng, How does the waterlogging regime affect crop yield? A global meta-analysis. *Front. Plant Sci.* **12**, 634898 (2021).
9. R. A. Ploschuk, D. J. Miralles, G. G. Striker, A quantitative review of soybean responses to waterlogging: Agronomical, morpho-physiological and anatomical traits of tolerance. *Plant Soil* **475**, 237–252 (2022).
10. EM-DAT, The International Disaster Database (2024); https://emdat.be/.
11. W. Kim, T. Iizumi, N. Hosokawa, M. Tanoue, Y. Hirabayashi, Flood impacts on global crop production: Advances and limitations. *Environ. Res. Lett.* **18**, 054007 (2023).
12. K. Liu, M. T. Harrison, H. Yan, D. L. Liu, H. Meinke, G. Hoogenboom, B. Wang, B. Peng, K. Guan, J. Jaegermeyr, E. Wang, F. Zhang, X. Yin, S. Archontoulis, L. Nie, A. Badea, J. Man, D. Wallach, J. Zhao, A. B. Benjumea, S. Fahad, X. Tian, W. Wang, F. Tao, Z. Zhang, R. Rötter, Y. Yuan, M. Zhu, P. Dai, J. Nie, Y. Yang, Y. Zhang, M. Zhou, Silver lining to a climate crisis in multiple prospects for alleviating crop waterlogging under future climates. *Nat. Commun.* **14**, 765 (2023).
13. Y. Li, K. Guan, G. D. Schnitkey, E. DeLucia, B. Peng, Excessive rainfall leads to maize yield loss of a comparable magnitude to extreme drought in the United States. *Glob. Change Biol.* **25**, 2325–2337 (2019).
14. K. G. Cassman, P. Grassini, A global perspective on sustainable intensification research. *Nat. Sustain.* **3**, 262–268 (2020).
15. Y. Hirabayashi, R. Mahendran, S. Koirala, L. Konoshima, D. Yamazaki, S. Watanabe, H. Kim, S. Kanae, Global flood risk under climate change. *Nat. Clim. Chang.* **3**, 816–821 (2013).
16. S. Zhang, L. Zhou, L. Zhang, Y. Yang, Z. Wei, S. Zhou, D. Yang, X. Yang, X. Wu, Y. Zhang, X. Li, Y. Dai, Reconciling disagreement on global river flood changes in a warming climate. *Nat. Clim. Chang.* **12**, 1160–1167 (2022).
17. J. Jägermeyr, C. Müller, A. C. Ruane, J. Elliott, J. Balkovic, O. Castillo, B. Faye, I. Foster, C. Folberth, J. A. Franke, Climate impacts on global agriculture emerge earlier in new generation of climate and crop models. *Nat. Food* **2**, 873–885 (2021).
18. R. P. Rötter, T. R. Carter, J. E. Olesen, J. R. Porter, Crop–climate models need an overhaul. *Nat. Clim. Chang.* **1**, 175–177 (2011).
19. C. Rosenzweig, J. Elliott, D. Deryng, A. C. Ruane, C. Müller, A. Arneth, K. J. Boote, C. Folberth, M. Glotter, N. Khabarov, K. Neumann, F. Piontek, T. A. M. Pugh, E. Schmid, E. Stehfest, H. Yang, J. W. Jones, Assessing agricultural risks of climate change in the 21st century in a global gridded crop model intercomparison. *Proc. Natl. Acad. Sci. U.S.A.* **111**, 3268–3273 (2014).
20. D. B. Lobell, G. L. Hammer, G. McLean, C. Messina, M. J. Roberts, W. Schlenker, The critical role of extreme heat for maize production in the United States. *Nat. Clim. Chang.* **3**, 497–501 (2013).
21. M. T. Harrison, Climate change benefits negated by extreme heat. *Nat. Food* **2**, 855–856 (2021).
22. W. Xie, W. Xiong, J. Pan, T. Ali, Q. Cui, D. Guan, J. Meng, N. D. Mueller, E. Lin, S. J. Davis, Decreases in global beer supply due to extreme drought and heat. *Nat. Plants* **4**, 964–973 (2018).
23. M. Gisbert-Queral, A. Henningsen, B. Markussen, M. T. Niles, E. Kebreab, A. J. Rigden, N. D. Mueller, Climate impacts and adaptation in US dairy systems 1981–2018. *Nat. Food* **2**, 894–901 (2021).
24. S. Beegum, D. Timlin, K. R. Reddy, V. Reddy, W. Sun, Z. Wang, D. Fleisher, C. Ray, Improving the cotton simulation model, GOSSYM, for soil, photosynthesis, and transpiration processes. *Sci. Rep.* **13**, 7314 (2023).
25. J. Eitzinger, M. Trnka, J. Hösch, Z. Žalud, M. Dubrovský, Comparison of CERES, WOFOST and SWAP models in simulating soil water content during growing season under different soil conditions. *Ecol. Model.* **171**, 223–246 (2004).
26. J. Zhou, G. Cheng, X. Li, B. X. Hu, G. Wang, Numerical modeling of wheat irrigation using coupled HYDRUS and WOFOST models. *Soil Sci. Soc. Am. J.* **76**, 648–662 (2012).
27. C. Rosenzweig, F. N. Tubiello, R. Goldberg, E. Mills, J. Bloomfield, Increased crop damage in the US from excess precipitation under climate change. *Glob. Environ. Change* **12**, 197–202 (2002).
28. J. Fu, Y. Jian, X. Wang, L. Li, P. Ciais, J. Zscheischler, Y. Wang, Y. Tang, C. Müller, H. Webber, B. Yang, Y. Wu, Q. Wang, X. Cui, W. Huang, Y. Liu, P. Zhao, S. Piao, F. Zhou, Extreme rainfall reduces one-twelfth of China's rice yield over the last two decades. *Nat. Food* **4**, 416–426 (2023).
29. S. Li, A. M. Tompkins, E. Lin, H. Ju, Simulating the impact of flooding on wheat yield—Case study in East China. *Agric. For. Meteorol.* **216**, 221–231 (2016).
30. X. Wang, Z. Liu, H. Chen, Investigating flood impact on crop production under a comprehensive and spatially explicit risk evaluation framework. *Agriculture* **12**, 484 (2022).
31. J. Han, Z. Zhang, J. Xu, Y. Chen, J. Jägermeyr, J. Cao, Y. Luo, F. Cheng, H. Zhuang, H. Wu, Q. Mei, J. Song, F. Tao, Threat of low-frequency high-intensity floods to global cropland and crop yields. *Nat. Sustain.* **7**, 994–1006 (2024).
32. IPCC, *Climate Change 2023: Synthesis Report. Contribution of Working Groups I, II and III to the Sixth Assessment Report of the Intergovernmental Panel on Climate Change*, Core Writing Team, H. Lee, J. Romero, Eds. (IPCC, 2023), pp. 35–115.
33. C.-S. Ma, B.-X. Wang, X.-J. Wang, Q.-C. Lin, W. Zhang, X.-F. Yang, J. van Baaren, D. P. Bebber, S. D. Eigenbrode, M. P. Zalucki, J. Zeng, G. Ma, Crop pest responses to global changes in climate and land management. *Nat. Rev. Earth. Environ.* **6**, 264–283 (2025).
34. G. Kaur, G. Singh, P. P. Motavalli, K. A. Nelson, J. M. Orlowski, B. R. Golden, Impacts and management strategies for crop production in waterlogged or flooded soils: A review. *Agron. J.* **112**, 1475–1501 (2020).
35. C. Zhao, B. Liu, S. Piao, X. Wang, D. B. Lobell, Y. Huang, M. Huang, Y. Yao, S. Bassu, P. Ciais, J.-L. Durand, J. Elliott, F. Ewert, I. A. Janssens, T. Li, E. Lin, Q. Liu, P. Martre, C. Müller, S. Peng, J. Peñuelas, A. C. Ruane, D. Wallach, T. Wang, D. Wu, Z. Liu, Y. Zhu, Z. Zhu, S. Asseng, Temperature increase reduces global yields of major crops in four independent estimates. *Proc. Natl. Acad. Sci. U.S.A.* **114**, 9326–9331 (2017).
36. J. Xu, C. Ren, X. Zhang, C. Wang, S. Wang, B. Ma, Y. He, L. Hu, X. Liu, F. Zhang, L. Lu, S. Li, J. Zhang, Y.-G. Zhu, P. Vitousek, B. Gu, Soil health contributes to variations in crop production and nitrogen use efficiency. *Nat. Food* **6**, 597–609 (2025).
37. B. Peng, K. Guan, J. Tang, E. A. Ainsworth, S. Asseng, C. J. Bernacchi, M. Cooper, E. H. Delucia, J. W. Elliott, F. Ewert, R. F. Grant, D. I. Gustafson, G. L. Hammer, Z. Jin, J. W. Jones, H. Kimm, D. M. Lawrence, Y. Li, D. L. Lombardozzi, A. Marshall-Colon, C. D. Messina, D. R. Ort, J. C. Schnable, C. E. Vallejos, A. Wu, X. Yin, W. Zhou, Towards a multiscale crop modelling framework for climate change adaptation assessment. *Nat. Plants* **6**, 338–348 (2020).
38. N. Alexandratos, Food price surges: Possible causes, past experience, and longer term relevance. *Popul. Dev. Rev.* **34**, 663–697 (2008).
39. R. Delzeit, F. Zabel, C. Meyer, T. Václavík, Addressing future trade-offs between biodiversity and cropland expansion to improve food security. *Reg. Environ. Change* **17**, 1429–1441 (2017).
40. P. Potapov, S. Turubanova, M. C. Hansen, A. Tyukavina, V. Zalles, A. Khan, X.-P. Song, A. Pickens, Q. Shen, J. Cortez, Global maps of cropland extent and change show accelerated cropland expansion in the twenty-first century. *Nat. Food* **3**, 19–28 (2022).

41. C. Reed, W. Anderson, A. Kruczkiewicz, J. Nakamura, D. Gallo, R. Seager, S. S. McDermid, The impact of flooding on food security across Africa. *Proc. Natl. Acad. Sci. U.S.A.* **119**, e2119399119 (2022).
42. M. Laber, P. Klimek, M. Bruckner, L. Yang, S. Thurner, Shock propagation from the Russia–Ukraine conflict on international multilayer food production network determines global food availability. *Nat. Food* **4**, 508–517 (2023).
43. F. A. Vogel, G. A. Bange, "Understanding USDA Crop Forecasts" (United States Department of Agriculture, 1999).
44. M. Glotter, J. Elliott, Simulating US agriculture in a modern Dust Bowl drought. *Nat. Plants* **3**, 1–6 (2016).
45. C. Daly, M. Halbleib, J. I. Smith, W. P. Gibson, M. K. Doggett, G. H. Taylor, J. Curtis, P. P. Pasteris, Physiographically sensitive mapping of climatological temperature and precipitation across the conterminous United States. *Int. J. Climatol.* **28**, 2031–2064 (2008).
46. H. Tian, J. Yang, C. Lu, R. Xu, J. G. Canadell, R. B. Jackson, A. Arneth, J. Chang, G. Chen, P. Ciais, S. Gerber, A. Ito, Y. Huang, F. Joos, S. Lienert, P. Messina, S. Olin, S. Pan, C. Peng, E. Saikawa, R. L. Thompson, N. Vuichard, W. Winiwarter, S. Zaehle, B. Zhang, K. Zhang, Q. Zhu, The global $N_2O$ model intercomparison project. *Bull. Am. Meteorol. Soc.* **99**, 1231–1251 (2018).
47. Food and Agriculture Organization of the United Nations (FAO), IIASA, ISRIC, ISS-CAS, JRC, Harmonized World Soil Database version 1.2, FAO (2012).
48. W. Shangguan, Y. Dai, Q. Duan, B. Liu, H. Yuan, A global soil data set for earth system modeling. *J. Adv. Model. Earth Syst.* **6**, 249–263 (2014).
49. F. T. Portmann, S. Siebert, P. Döll, MIRCA2000—Global monthly irrigated and rainfed crop areas around the year 2000: A new high-resolution data set for agricultural and hydrological modeling. *Global Biogeochem. Cycles* **24**, B1011 (2010).
50. D. Yamazaki, D. Ikeshima, R. Tawatari, T. Yamaguchi, F. O'Loughlin, J. C. Neal, C. C. Sampson, S. Kanae, P. D. Bates, A high-accuracy map of global terrain elevations. *Geophys. Res. Lett.* **44**, 5844–5853 (2017).
51. D. Yamazaki, D. Ikeshima, J. Sosa, P. D. Bates, G. H. Allen, T. M. Pavelsky, MERIT Hydro: A high-resolution global hydrography map based on latest topography dataset. *Water Resour. Res.* **55**, 5053–5073 (2019).
52. D. Yamazaki, S. Kanae, H. Kim, T. Oki, A physically based description of floodplain inundation dynamics in a global river routing model. *Water Resour. Res.* **47**, W04501 (2011).
53. D. Yamazaki, H. Lee, D. E. Alsdorf, E. Dutra, H. Kim, S. Kanae, T. Oki, Analysis of the water level dynamics simulated by a global river model: A case studyin the Amazon River. *Water Resour. Res.* **48**, W09508 (2012).
54. D. Yamazaki, T. Sato, S. Kanae, Y. Hirabayashi, P. D. Bates, Regional flood dynamics in a bifurcating mega delta simulated in a global river model. *Geophys. Res. Lett.* **41**, 3127–3135 (2014).
55. J. Muñoz-Sabater, E. Dutra, A. Agustí-Panareda, C. Albergel, G. Arduini, G. Balsamo, S. Boussetta, M. Choulga, S. Harrigan, H. Hersbach, B. Martens, D. G. Miralles, M. Piles, N. J. Rodríguez-Fernández, E. Zsoter, C. Buontempo, J.-N. Thépaut, ERA5-land: A state-of-the-art global reanalysis dataset for land applications. *Earth Syst. Sci. Data* **13**, 4349–4383 (2021).
56. X. Zhou, C. Prigent, D. Yamazaki, Toward improved comparisons between land-surface-water-area estimates from a global river model and satellite observations. *Water Resour. Res.* **57**, e2020WR029256 (2021).
57. F. Papa, C. Prigent, F. Aires, C. Jimenez, W. B. Rossow, E. Matthews, Interannual variability of surface water extent at the global scale, 1993–2004. *J. Geophys. Res. Atmos.* **115**, D12111 (2010).
58. Y. Dai, Q. Xin, N. Wei, Y. Zhang, W. Shangguan, H. Yuan, S. Zhang, S. Liu, X. Lu, A global high-resolution data set of soil hydraulic and thermal properties for land surface modeling. *J. Adv. Model. Earth Syst.* **11**, 2996–3023 (2019).
59. R. W. Webb, C. E. Rosenzweig, E. R. Levine, Global Soil Texture and Derived Water-Holding Capacities (Webb et al.), version 1, ORNL Distributed Active Archive Center (2000); https://doi.org/10.3334/ORNLDAAC/548.
60. R. L. Jones, A. Kharb, S. Tubeuf, The untold story of missing data in disaster research: A systematic review of the empirical literature utilising the Emergency Events Database (EM-DAT). *Environ. Res. Lett.* **18**, 103006 (2023).
61. X. Wang, X. Meng, Y. Long, Projecting 1 km-grid population distributions from 2020 to 2100 globally under shared socioeconomic pathways. *Sci. Data* **9**, 563 (2022).



**Acknowledgments**

**Funding:** This study was supported by the Guangdong Major Project of Basic and Applied Basic Research (no. 2021B0301030007), the National Key Research and Development Program of China (no. 2023YFF0804904), the National Natural Science Foundation of China (no. 42575173), the Fundamental and Interdisciplinary Disciplines Breakthrough Plan of the Ministry of Education of China (JYB2025XDXIM902), and the Fundamental Research Funds for the Central Universities, Sun Yat-sen University (no. 241gqb007). **Author contributions:** Conceptualization: S.Z., L.Z., and Y.D. Methodology: S.Z. and L.Z. Software: S.Z. Validation: S.Z., and H.L. Formal analysis: S.Z. Investigation: S.Z. and H.L. Resources: Y.D. Data curation: S.Z., H.L., and O.O. Writing—original draft: S.Z. and L.Z. Writing—review and editing: S.Z., L.Z., H.L., and Y.D. Visualization: S.Z., O.O., and H.L. Supervision: Y.D. Project administration: Y.D. Funding acquisition: S.Z. and Y.D. **Competing interests:** The authors declare that they have no competing interests. **Data, code, and materials availability:** County-level yield and harvest area in the US were obtained from the Department of Agriculture National Agricultural Statistics Service (https://quickstats.nass.usda.gov/). Crop insurance data were obtained from the US Department of Agriculture's Risk Management Agency (https://legacy.rma.usda.gov/data/cause.html and https://www.rma.usda.gov/tools-reports/summary-of-business). Daily precipitation data were obtained from PRISM (https://prism.oregonstate.edu/). The ERA5-Land dataset is available at https://ecmwf.int/en/era5-land. A global dataset of soil hydraulic parameters was provided by http://globalchange.bnu.edu.cn/research/soil5.jsp, and the Global Soil Texture and Derived Water-Holding Capacities dataset was obtained from https://daac.ornl.gov/SOILS/guides/WebbRosenzweig.html. Global gridded harvest area data for each crop were sourced from https://zenodo.org/records/7422506. Crop prices were obtained from the FAO statistical database (www.fao.org/faostat/en/#data/PP). The Emergency Events Database can be accessed from https://public.emdat.be/. Outputs of global crop and hydrologic models participating in the Inter-Sectoral Impact Model Intercomparison Project 3 were available at https://data.isimip.org/search/. The global gridded dataset for gross domestic product (GDP) was obtained from https://doi.org/10.5061/dryad.dk1j0. A global gridded population dataset was provided by https://doi.org/10.6084/m9.figshare.19608594.v2. The code for the global hydrodynamic model CaMa-Flood is available from https://hydro.iis.u-tokyo.ac.jp/~yamadai/cama-flood/. All data and code needed to evaluate and reproduce the results in the paper are present in the paper and/or the Supplementary Materials. This study did not generate new materials.

Submitted 21 October 2025
Accepted 12 March 2026
Published 15 April 2026
10.1126/sciadv.aed2754

# Underestimated agricultural losses due to flooding

Shulei Zhang, Liming Zhou, Hongbin Liang, Omarjan Obulkasim, and Yongjiu Dai

*Sci. Adv.* **12** (16), eaed2754. DOI: 10.1126/sciadv.aed2754



*Science Advances* (ISSN 2375-2548) is published by the American Association for the Advancement of Science. 1200 New York Avenue NW, Washington, DC 20005. The title *Science Advances* is a registered trademark of AAAS.